City Research Online

City, University of London Institutional Repository

Graphene-Carbon Composites for Solar and Low-voltage Powered Efficient Interfacial Evaporation

Fenghua Liu, Lijian Wang, Robert Bradley, Binyuan Zhao* and Weiping Wu*

F. Liu, L. Wang, Prof. B. Zhao
State Key Laboratory of Metal Matrix Composites,
School of Materials Science and Engineering,
Shanghai Jiao Tong University,
Shanghai, 200240, China

Prof. R. Bradley
Department of Materials, University of Oxford,
16 Parks Road, Oxford, OX1 3PH, United Kingdom
MatSurf Technology Ltd.
The Old Stables Marion Lodge, Little Salkeld, Penrith,
Cumbria, CA10 1NW, United Kingdom

Dr. W. Wu
Department of Electrical and Electronic Engineering,
School of Mathematics, Computer Science and Engineering,
City, University of London,
Northampton Square, London, EC1V 0HB, United Kingdom

Corresponding Authors

*Email: byzhao@sjtu.edu.cn

*Email: Weiping.Wu@city.ac.uk

Abstract

Nanocarbon materials have great potential for sustainable energy harvest and energy utilizations, such as solar thermal stream generation and interfacial evaporation. However, the evaporation rate is far too low for practical application. The technologies are not ready yet for industries requiring rapid, energy efficient and low cost evaporation processes such as distillation and sterilization. In this paper, flexible ultrathin graphene-carbon cloth (CC) based carbon-carbon composites have been prepared by in-situ electrochemical reduction of graphene oxide (rGO). The carbon-carbon composite materials demonstrated high performance in photothermal evaporation, more importantly, the all carbon-based devices can also be operated as low voltage Joule heating elements in wide temperature range up to 389 °C. Even with a very low voltage 3 V applied, the graphene-CC heater can reach a very high with very high heating speed up to 112 °C/sec, and a steady-state temperature up to 292 °C within 10 seconds only. The low voltage heater promises as the most effective solution for high-speed interfacial evaporations, its evaporation rate can reach upto 45.87 kg m^{-2} h^{-1}, enhanced by one order of magnitude compared to the best solar power photothermal seawater desalination devices ever reported.

In recent years, nano carbon materials have shown attractive ability in the fields of photothermal utilization and interface evaporation, due to their wide spectral absorption capacity and suitable adjustable porous structure.[1-5] The factors affecting the interface evaporation are input energy, mass transfer and thermal management. Among them, many scholars have done a lot of work in thermal management, but there is still insufficient research on the surface properties and other types of that can be adapted for higher speeds of interface evaporation.[6-10] In terms of energy utilization, the direct use of sunlight is very cost effective, but the evaporation rate that can be achieved is limited due to the relative low energy density of solar illumination[11]. Therefore, devices solely powered by solar energy, are not suitable for practical and industrial applications that require high-speed evaporations such as distillations, purification, sterilization, and so on.[12] The cost of using nano materials or optical devices to enhance the illumination intensity will be very high Joule heating (or thermal effect of current), is the most fundamental and useful property of electricity, is promising, robust and useful for these sustainable energy harvest and energy utilization systems.

Flexible heaters have also been one of the hotspots of the research on functional materials in recent years, due to their high heating efficiency, light weight and superior mechanical properties. They have been used for wearable electronics, hot plates, electric blankets, smart windows and so on. Various metals, alloys, conductive oxides have been exploited as the active materials for heating elements, examples include silver nanowires,[13-15] Cu-Ni micromesh,[16] Fluorine-doped Tin Oxide (FTO),[16] Gallium (Ga) doped Zinc Oxide (GZO) thin films[17] and so on. Conductive nanocarbon materials can be designed as the Joule heating elements and systems to establish the next generation of sustainable thermal processes and heating systems. Carbon materials including carbon nanotubes (CNTs),[18-20] Graphene,[21] exfoliated graphite,[22] laser reduced GO,[23] are promising materials due to their low cost, mechanical flexibility, superior electrical conductivity and high efficiency. Graphene exhibits excellent performance in electrical heating due to its high electrical conductivity, high mechanical strength and high thermal conductivity.[24, 25] However, these materials are not mechanically or chemically stable enough. Besides, the heating devices with these materials require

a higher driving voltage to achieve high temperature, which can cause severe safety and operability problems. Besides, the thermal responses are still too slow. Most of previous studies have been mainly focusing on the using a single form of carbon materials or relying on a single function. The electric energy is a stable energy source, which can be integrated with a wide range of power grid and infrastructures, besides, electricity can eanble new operations with a variety of physics and electronics, such as magenetic, microwave, sensors towards smart energy havest and storage systems.

In the conventional evaporation and distillation, the solution is often heated to boiling point, which is energy-intensive but not optimized or efficient, due to related limited fixed size of interface area and a low amount of liquid being treated. The use of micro-nano structures to achieve interface evaporation, can effectively reduce the energy consumption and not affected by the volume of the solution being processed.[11] In addition, the surface properties of the nano material, especially the hydrophobicity and hydrophilic, has greater impacts on the interface evaporation. Hydrophilic materials can rapidly transfer solution to the hot zone by capillary, but the ideal evaporating layer acts as the zone of local limitation of heat and reaction for interfacial evaporation is necessary, to avoid the adsorption of excess water and cause energy loss.[26] In order to achieve higher rate of interface evaporation, in this paper, we proposed and sucessfully demostrated the graphene-carbon composite materials as both a high-rate solar evaporation device and a novel, low-voltage driven electrical heater as the energy source of steam geneartion and distillation for the first time.

Flexible reduced graphene oxide composited with carbon cloth (rGO-CC), prepared by electrochemical deposition and in-situ Joule heat reduction induced by electrical field, have been sucessfully used as solar and electric heaters for pure water production by efficient evaporation powered by clean energy. The properties of materials, the impact of hydrophilicity/hydrophobicity, the electrothermal performances and the water evaporation efficiency were studied thoroughly.

In the electrochemical deposition, shown in **Figure 1**a, the GO was dispersed in deionized water and then stirred uniformly to obtain an aqueous solution with the concentration of 0.5 mg mL^{-1}. A

piece of carbon cloth and a platinum plate were used as the positive and the negative electrode, respectively. These two electrodes were kept facing each other with the space about 2 centimeters.
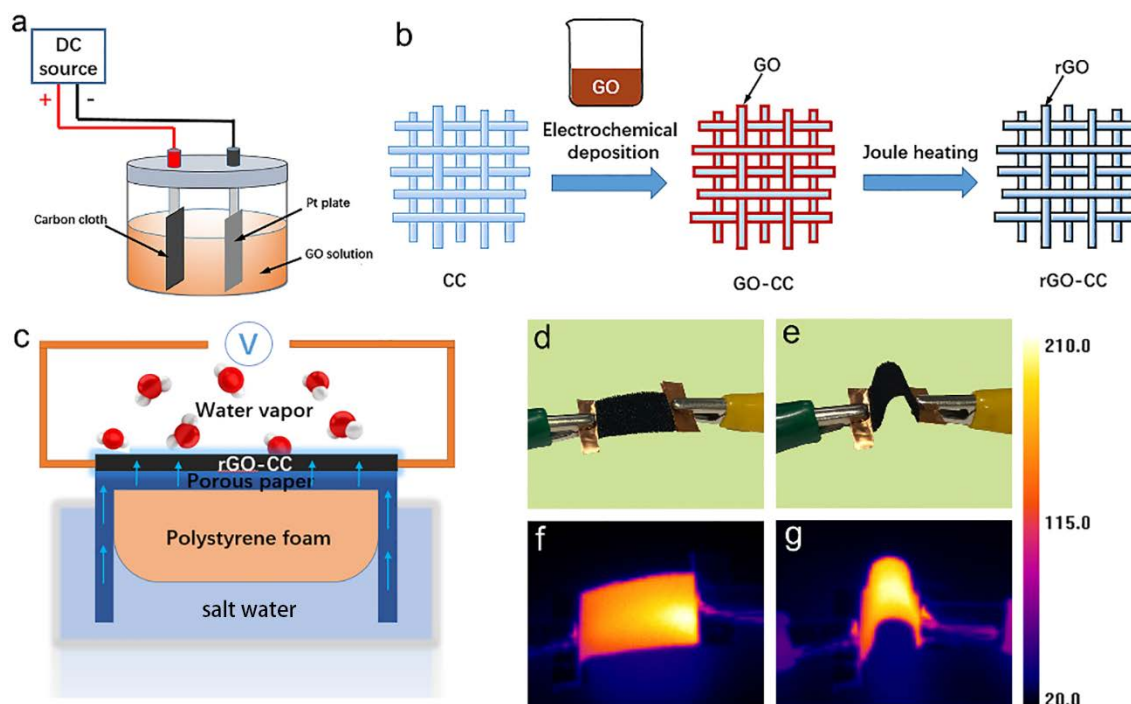

Figure 1. The preparation of GO-CC and rGO-CC composites. a) The electrochemical deposition of graphene. b) The schematic diagram of electrochemical deposition and Joule heating process to obtain rGO on carbon cloth samples. c) The schematic diagram of rGO-CC composite heating elements to generate water vapour with low voltage. d-g) The photographs and infrared photos of the rGO-CC (flat and bending).

Figure 1b shows a schematic diagram of the fabrication procedures. The GO-CC sample was obtained by the electrochemical deposition with the applied voltage of 5 V for 4 hours. After that, the sample was dried in a vacuum oven at room temperature overnight. After that, the reduction of GO was achived by Joule heating with the power generated by applying a 3 V voltage to the GO-CC sample for 5 minutes under Ar atmosphere. The photograph of the rGO-CC sample obtained which is shown in Figure S1. A schematic diagram of efficient water evaporation device using the composite material is shown in Figure 1c. The polystyrene foam is used as the floating and supporting substrate, and two-dimensional flexible porous hydrophilic paper served as the water guiding media, which is responsible for transferring the bottom salt water to the upper layer. The porous paper is in intimate

contact with the top rGO-CC layer by physical methods. A low voltage is applied on the rGO-CC to obtain a high temperature in the open air environment, and the water conducted to the upper portion can be rapidly heated and converted into vapor. This composite material has superb thermal conductivity and electrical conductivity, coupled with excellent flexibility. As being shown in Figure 1d-1g, the rGO-CC exhibits good electrothermal performances at low voltages. High temperature, homogenes and large area thermal field can be achieved in both straight and curved configiations.

The surface morphologies of CC, GO-CC and rGO-CC are exhibited in **Figure 2** and Figure S2. The clean fibers of the CC with diameter of about 10 μm could be clearly identified in Figure 2a. The GO surface on CC is relatively smooth and flat with slight thin curls at the edges, which confirmed that the small number of GO layers (Figure 2b, c). However, in Figure 2d and 2e, it can be found that the rGO reduced by Joule heat have been tightly coated on the carbon fibers, showing obvious folds at the edges and lots of wrinkles in the middle plate. The rGO coated on CC just behaves like pieces of paper on 1D column arrays and most of them showing translucent features at the end of the edges (Figure 2f). In addition, the compositing structures have extra spaces filled by air, due to the gap between the 2D graphene and the column shaped carbon fibers (Figure 2e and Figure S2). Since the oxygen-containing functional groups of the GO were reduced during Joule heating, the rGO sheets agglomerated and overlapped with each other. Due to the high temperature of the Joule heating process and the rapid heating rate, a lot of cracks formed in the rGO. When the voltage was applied, the temperature raised rapidly, and the thermal energy generated can destroy carbon-oxygen bonds forming CO or CO_2.[27, 28] The rapid release of the gases caused the expansion of the graphene layers in the vertical direction, and the rGO became thicker and denser compared with the GO.
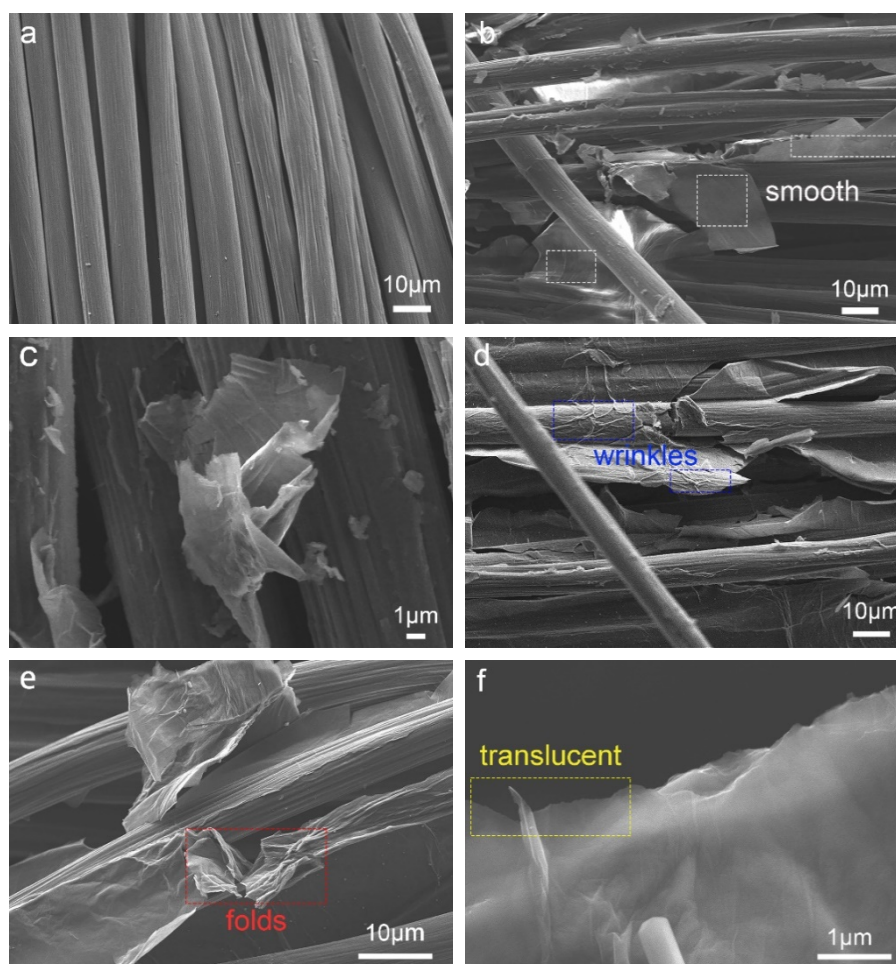
Figure 2. Typical SEM photographs. a) The surface morphologies of CC. b, c) The flat and smooth GO were coated on CC by electrochemical deposition. d-f) The rGO was tightly coated on fibers of CC and showed much wrinkles which was reduced by Joule heating.

The X-ray Diffraction (XRD) patterns of the CC, GO-CC and rGO-CC materials are illustrated in **Figure 3**a and Figure S3. It can be seen that compared to the CC, the XRD peak of the GO-CC obtained by electrochemistry depositing of graphene oxide on CC and the XRD peak of rGO-CC reduced by Joule heating have not changed much, and all of them have the same strong diffraction peaks around $2\theta = 26°$ corresponding to the (002) reflection of carbon corresponding to the stacking structures of aromatic layers. In the XRD pattern of GO-CC, a weak diffraction peak of graphite oxide (001) can be detected.

The Raman spectrum of these carbon composites are shown in Figure 3b, the D peak at 1344 cm^{-1} and the G peak at 1588/1575 cm^{-1} are conspicuous in all samples. The number of defects and the degree of disorder are direct evidences of the degree of graphitization, which can be easily evaluated

by the intensity ratio of I_D/I_G.[25] This ratio is the lowest in CC, indicating that CC has the highest degree of graphitization. As the GO deposited on CC and then reduced by thermal, the ratio gradually increased, indicating that the defects and structure disorder were obviously increased and the thermal reduction induced plenty of defects after partial removal of functional groups.[29]
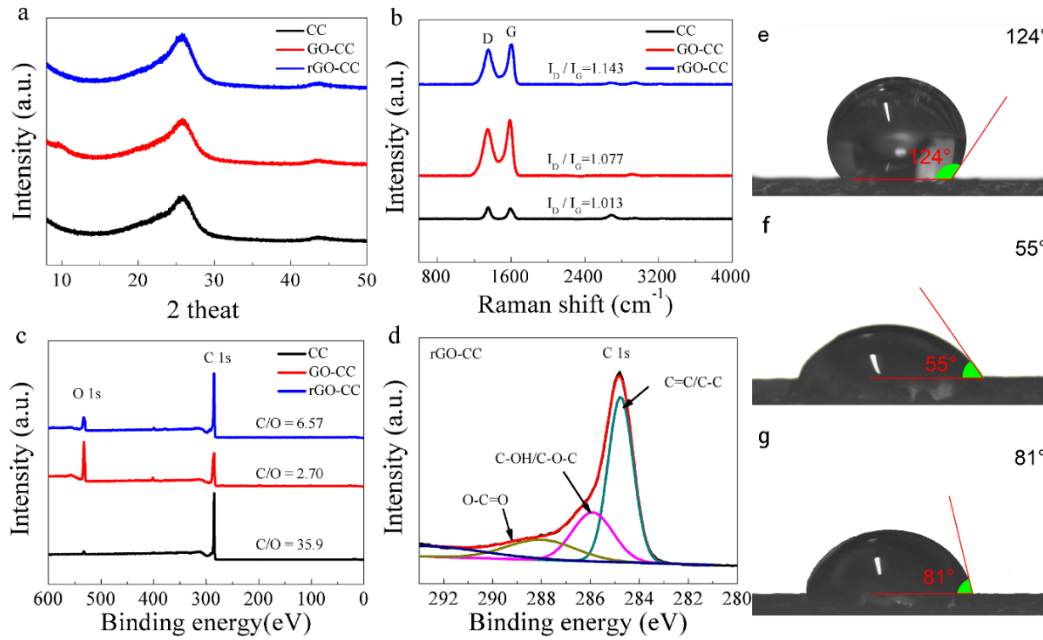

Figure 3. The characterization of CC, GO-CC and rGO-CC. a) The XRD patterns, b) The typical Raman spectrum, c, d) The X-ray photoelectron spectroscopy (XPS) results of CC, GO-CC and rGO-CC samples. e-g) The contact angles of a DI water drop on the CC, GO-CC and rGO-CC samples, respectively.

In order to analyze the elemental valence states of the above three materials, X-ray photoelectron spectroscopy (XPS) was used to analysis the samples. The contents of oxygen (O) in CC, GO-CC and rGO-CC were 3.6 at%, 30.6 at% and 16 at%, respectively. Simultaneously, the oxygen content of the CC is very low, so the atomic ratio of carbon to oxygen (C/O) is also very large (C/O=35.9). The prepared GO-CC contains a large amount of oxygen-containing functional groups with a C/O ratio of 2.7. After the heat reduction, the oxygen-containing functional groups were partially removed, and the O 1s peak of the rGO-CC decreased and the C/O ratio increased to 6.57. The fitting peaks of C 1s from XPS spectra shows that the presence of C=C/C-C (284.8 eV), C-O (285.6 eV) and O=C-O (287.8 eV) functional groups are about 87.5%, 9.6% and 2.9%, respectively (Figure 3d and Figure

S4a, S4b). The hydrophilicity of the three materials was tested. As being shown in the Figure 3e-3g, the contact angles of the CC, GO-CC, rGO-CC were 124 °, 55 ° and 81 °, respectively, indicating that the hydrophobicity of CC and the hydrophilicity of GO-CC is the best.

The evaporation rate of photothermal devices under normal solar irradiation (1 kWm^{-2}) is a key indicator and figure of merit for applications. Hydrophobic CC, GO-CC prepared by electrodeposition and rGO-CC obtained by in situ reduction of Joule heat, were used to test the effect of photothermal evaporation, as shown in **Figure 4**. Both rGO-CC and GO-CC are superior to CC in optical absorption, the absorption in the ultraviolet and visible regions are as high as 97.2% and 96.9% (280 nm-760 nm, CC 93.4%), and 93.6% and 93.1% in the near-infrared region (760 nm-2500 nm, CC 89.2%), respectively. (Figure 4a).

Under the illumination of 1 kWm^{-2}, as shown in Figure 4b, the steady state evaporation rate of rGO-CC reached 2.54 kg m^{-2} h^{-1}, which is 5 times that of natural evaporation (0.51 kg m^{-2} h^{-1}). The evaporation rate of hydrophobicity CC is 2.4 kg m^{-2} h^{-1}, which is better than GO-CC (2.34 kg m^{-2} h^{-1}). This should be due to the fact that GO-CC contains a large amount of oxygen-containing functional groups and is hydrophilic (Figure 3c-3g), which make it absorbing more aqueous solution, and lose much heat. The hydrophobic CC absorbs sunlight and converts it into heat and the porous cloth which is in close contact with the bottom of CC is heated to evaporation. The macroscopic pores of CC are large, and it is favorable for the escape of water vapor, so the evaporation rate is high. The temperature change can also be found during the evaporation recorded by the infrared camera in real time. The average surface temperature of the hydrophilicity GO-CC device is the lowest, about 38.5 °C. Due to the strong solar absorption, the rGO-CC with less hydrophilic has an average surface temperature of 41 °C (Figure 4c). We tested the stability of these devices and performed multiple cycles, each for more than 1 hour. The average evaporation rate is shown in Figure 4d. It can be seen that the evaporation rate after long-term operation is relatively stable.
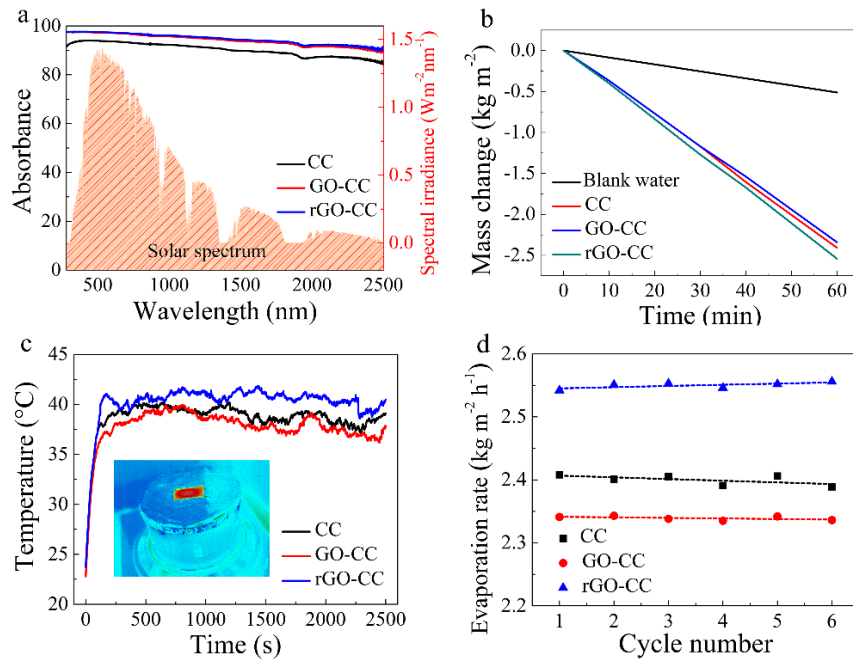
Figure 4. Typical photothermal performances in water evaporation (1 kW m^{-2}). a) The solar energy absorption, b) Mass change as a function of time, c) The average temperature as a function of time, d) The cycle performances on water evaporation rate of CC, GO-CC and rGO-CC, respectively.

The electrothermal performance of the flexible rGO-CC heating elements were studied carefully shown in **Figure 5**. After the power (3V) was turned on, the temperature of the flexible heaters (CC, GO-CC and rGO-CC) rised rapidly over time and then reached the steady state temperature 269 °C, 150 °C and 298 °C, respectively, showed in Figure 5a. When the power was disconnected, the temperature droped rapidly to room temperature. Among them, GO-CC and rGO-CC reached the steady state within 10 seconds, while the CC heater can acheive a high temperature around 10 seconds, but the temperature was still in a slow rising state before the power was turned off. According to the formula P=U^2/R (where P is the power, U is the applied voltage, and R is the resistance), the rGO-CC reached the highest temperature at voltage of 3 V which can attributed to its lowest resistance. The temperature versus time curves of rGO-CC at different applied voltages ranged from 0.5 V to 3 V are showed in Figure 5b, and the temperature reached the steady state of 30.9 °C, 56.7 °C, 107.9 °C, 157.3 °C, 226.4 °C and 299.6 °C within about 10 seconds, respectively. As the applied voltages on the same piece of rGO increased, the resistance gradually decreased and the power increased exponentially (Figure 5c). Graphene oxide (GO) is a layered compound with large interlayer distances

obtained by deep oxidation of graphite in the liquid phase. There are a large number of polar groups in GO-CC. With the Joule heating, the interlayer water is desorbed and the oxygen-containing group is decomposed. With the heating temperature rise, the interlayer distance decreases rapidly, and the electrical conductivity gradually increases. However, the reduction by the Joule thermal has not yet reached the graphite-like state due to the low temperature. As the temperature rises, the rGO-CC will still translate to the graphite-like state, and the electrical conductivity also increases. The steady temperature and the heating rate are liner with the applied power, as shown in Figure 5d. The temperature reached 389 °C and the heating rate achieved as high as 82 °C per second, respectively.

The cycle stability at low voltage 3V of the rGO-CC is shown in Figure 5e, and the performances are very stable. The temperature rised rapidly and stabilized after the voltage was applied, and droped fast to room temperature when the power was turned off, indicating that the electrical properties of the flexible heater are relatively stable especially during the application of voltage and heat generation. Although the temperature that the heater can reach is directly determined by the input power rather than the resistance, the input voltage of the heater with low resistance is relatively small when the same power is input, which is very important for practical applications. The low voltage can be achieved with simple equipment and at high level of safety, so the applications will be wider. In addition, the thermal conductivity of the rGO-CC is excellent, so the response time of the temperature is very short. The high steady-state temperature and the fast response are both very important for heaters, allowing the heaters extend their applications enormously. The steady-state temperature (389 °C) and fast response (10 s) of the rGO-CC flexible heater achieved at a low driving voltage (3.5 V) , as shown in Figure 5f.
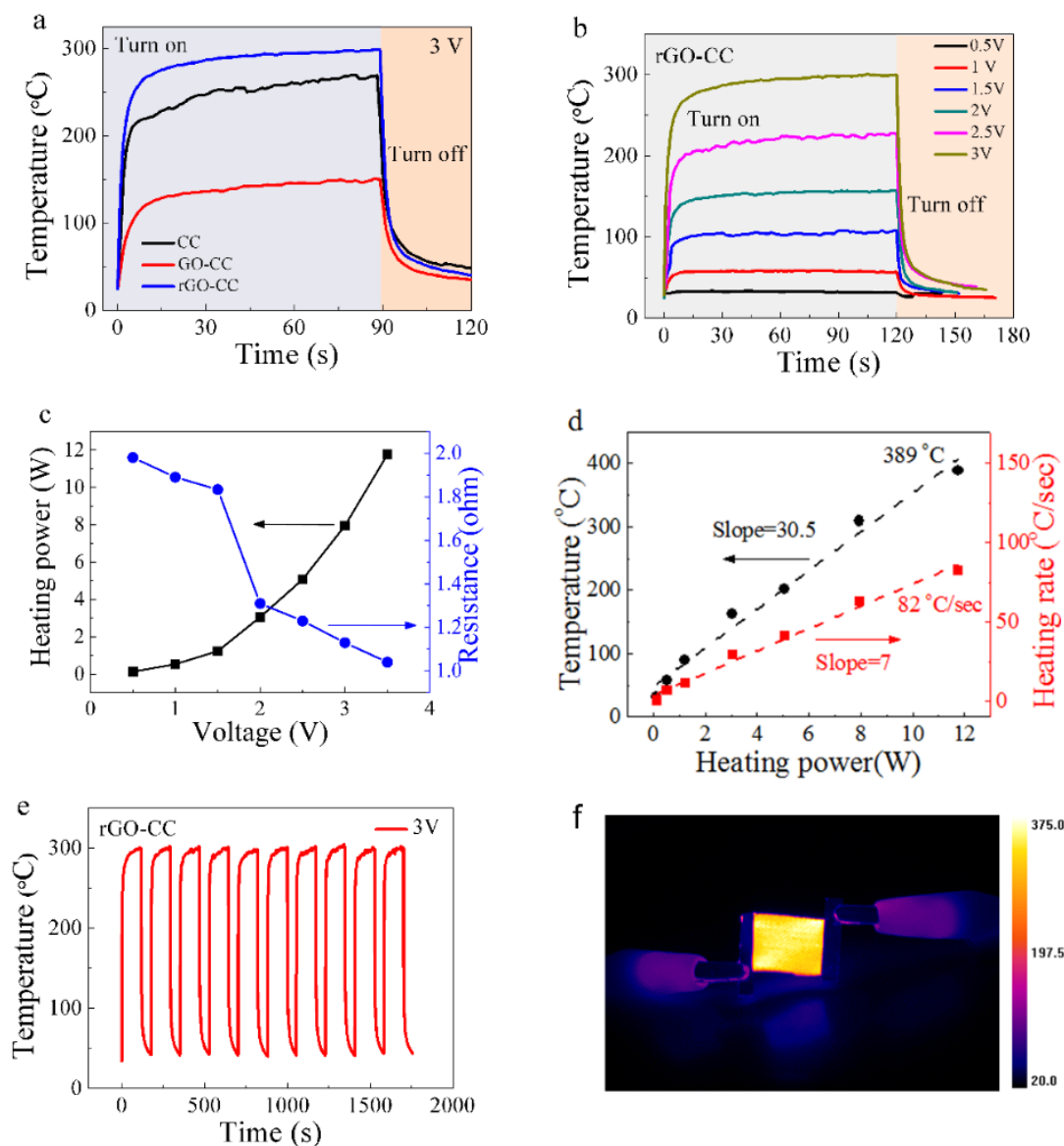
Figure 5. Typical electrical and electrothermal properties. a) Surface temperature-time curves of CC, GO-CC and rGO-CC at the low voltage (3V). b) The temperature-time curves of rGO-CC at different voltages. c) The heating power and resistance of the rGO-CC at different voltages. d) The curves of temperature rise and average heating rate of rGO-CC as the power increases. e) The electrothermal cycle performance of the rGO-CC at 3 V. f) The infrared (IR) photo of the rGO-CC device applied a voltage of 3.5 V.

With the help of Joule heating elements CC (hydrophilic/hydrophobic), GO-CC and rGO-CC, steam and fresh water can be produced from the saline water efficiently with low voltage power sources. **Figure 6**a and Figure S5 show the evaporation rate under different applied voltages. The evaporation rate of the rGO-CC reached 1.75, 8.04, 26.92 kg m^{-2} h^{-1} with the voltage of 1 V, 2 V and

3 V, respectively. While the hydrophobic CC showed more profound performance, and the water evaporation rate reached 45.87 kg m^{-2} h^{-1} at voltage of 3 V (Figure 6b). The GO-CC and hydrophilic CC behavied similar performance which reached 26.79 and 25.04 kg m^{-2} h^{-1}, respectively. Although the dried rGO-CC exhibited higher temperature performance at the same voltage due to the decrease in electrical resistance, it still exhibited hydrophilicity which contained a large amount of hydrophilic functional groups and showed the similarly performance in water evaporation as well as GO-CC and hydrophilically modified CC. Comparing the evaporation rates at different voltages, the water evaporation rate of the four heaters at 1 V and 2 V was similarly shown in Figure 6c. However, GO-CC, rGO-CC and hydrophilically modified CC behaving hydrophilia can absorb much water and the evaporation rate is greatly limited at 3 V. The infrared photos of the rGO-CC device, shown in Figure 6g-j, indicated the process of the energy distribution. Due to the difference of the hydrophilicity, even at the same applied voltage, the average surface temperature and heat distribution of these three devices were different, as shown in Figure S6 and S7. The hydrophobic CC can maintain direct connection with the thin water rather swallow much water in the body, so the water molecules at the surface can be heated and evaporate rapidly under high temperature.

The ratio of evaporation rate to applied power is also compared with different heaters and different voltages, shown in Figure 6d. The GO-CC heater was relatively stable, and the ratio increases linearly with voltage increase. The ratio of the hydrophilic modified CC was lower than other heaters. The rGO-CC and hydrophobic CC kept relatively constant at 1 V and 2 V, while the gap becomes larger at 3 V with the performance of CC 4.68 and rGO-CC 4.17 kg m^{-2} h^{-1} W^{-1}. At low voltage, the water evaporation rate is substantially linear with the input voltage, and the ratio of evaporation rate to inputp ower of these heaters are also close except for hydrophilic CC. However, the water evaporation rate of hydrophobic CC is about 1.8 times of other heaters under 3 V. It indicates that the hydrophilicity increases the electrical resistance to a certain extent, resulting in a slight decrease of the input power, but more importantly, the hydrophilic heater has a strong ability to capture water molecules, which resulted in more water molecules be heated simultaneously and can not easily

escape. Since the hydrophobic heater maintains its own conductivity and the water molecules are easily heated and escaped from the hot zone of the heater, the hydrophobic heaters can achieve faster water evaporation rates.
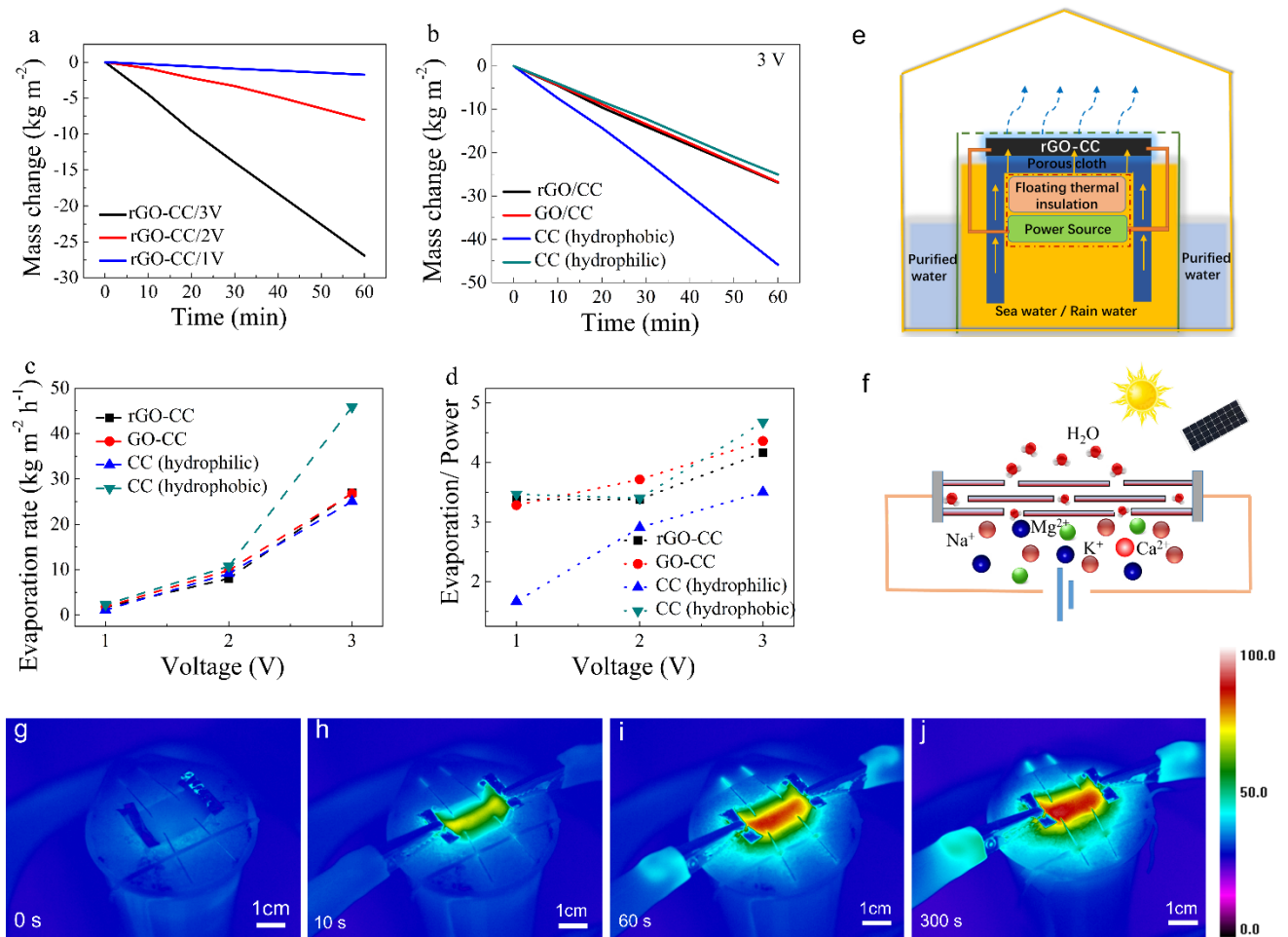
Figure 6. The performance of Joule heating elements in water evaporation. a) Mass change of the rGO/CC at different voltages. b) The water evaporation of the CC, GO-CC and rGO-CC at voltage of 3 V. c) The evaporation rate curves of the CC, GO-CC and rGO-CC at different applied voltages. d) The ratio of evaporation rate to applied power at different voltages. e, f) The schematic diagram of generating water vapour and desalination via Joule heating, respectively. g-j) The infrared (IR) photos of the rGO-CC device operated under the voltage of 3 V which were taken at 0 s, 10 s, 60 s and 300 s (steady state).

The energy conversion efficiency (η) is used as a measure to evaluate the electric energy-to-vapor efficiency. The formula is defined as,

$$\eta = \frac{m h_{LV}}{P_{input} t} \tag{1}$$

where m is the mass loss rate per unit area calculated from the slop of mass loss curves at the steady state, h_{LV} is the total enthalpy of sensible heat (315 J g^{-1}, from ca. 25 °C to 100 °C with specific heat of water 4.2 J g^{-1} K^{-1}) and liquid-vapor phase change (2256 J g^{-1}). P_{input} is the input power by Joule heating and t is the running time. As the voltage increases, the energy conversion efficiency gradually increases. The energy conversion efficiency of the hydrophobic CC of 3V is 80.2% (Table S1). We also tested different samples size (4×2 cm), as shown in the Figure S8. After the sample was enlarged, the electrothermal conversion and the Joule heat evaporation performance slightly decreased, but basically maintained a high evaporation rate.

We designed a device (Figure 6e) to achieve rapid evaporation of water with low voltage and to collect fresh water. Since the temperature was lower than 100 °C (Figure S7), only water molecules in the brine were heated to vapor, and most of the ions were still in the brine (Figure 6f). The effect of desalination was carefully examined, and the concentration of the primary ions were extramely eliminated (Figure S9). After desalination, the calcium ions, potassium ions, magnesium ions and sodium ions decreased from 9,942 mg L^{-1}, 1168 mg L^{-1}, 8,018 mg L^{-1} and 11,210 mg L^{-1} to 1.2 mg L^{-1}, 0.21 mg L^{-1}, 8.1 mg L^{-1} and 8.5 mg L^{-1}, respectively.

To summarize, we have developed a new versatile, flexible concept that combines both photothermal and low-voltage heating elements. The solar absorption can reach 97%-93%, and the evaporation rate of rGO-CC can reach 2.54 kg m^{-2} h^{-1} under normal illumination of 1 kWm^{-2}. These heating elements achieved higher temperature at lower voltage inputs. Among them the rGO-CC heater reached 309 °C at 3 V (389 °C at 3.5 V), and the temperature response time was only 10 seconds indicating good conductivity and thermal conductivity. These porous heaters also have good effect on water evaporation. Although the conductivity and heat transferability of the dried rGO-CC

is higher, the hydrophilicity causes more immersion of water, which in turn changes the electrical conductivity of the whole device. The hydrophilic heaters can absorb more water, resulting all these water molecules be heated simultaneously not vaporized in time under low input power. The hydrophilic binding force of water molecules is large, which hinders the escape of water molecules. Hydrophilic materials have a stronger binding force on water molecules and also hinder the rate of water evaporation to some extent. While the hydrophobic CC heater can produce more heat at the same voltage. Therefore, in terms of electric heating to achieve interfacial evaporation, the water evaporation rate of hydrophilic carbon (rGO-CC) and the hydrophobic carbon can reach first-rank interfacial evaporation rate upto 27 kg m^{-2} h^{-1} and 45.87 kg m^{-2} h^{-1}, respectively. The flexible porous conductive materials utilizing low-voltage electricity to achieve rapid water evaporation that is one order of magnitude higher compared to the best solar powered seawater desalination devices reported.[26] Our new carbon-carbon materials and devices promise a bright future as an emergency solution for the lack of clean drinking water sources in dry areas, the production of purified fresh water in extreme conditions, and the most reliable sources of water supply for the space explorations.

Experimental Section

Materials: Sodium chloride (NaCl), potassium chloride (KCl), magnesium sulfate ($MgSO_4$), calcium chloride ($CaCl_2$) and graphite were provided by Sigma-Aldrich. The electrical resistivity of the deionized water was 18.2 $M\Omega\cdot cm$. The carbon cloth (CC) samples were purchased from Fuel Cell Earth.

Fabrication of GO-CC, rGO-CC and hydrophilic CC materials: Typically, the graphene oxide (GO) were prepared by the modified Hummers method.[30] The GO-CC samples were prepared by electrophoretic deposition in 50 ml GO suspension with the concentration of 0.5mg ml^{-1} at an applied voltage of 5 V for 4 hours. The CC (2×3 cm) was used as the positive electrode. Using a piece of Pt and a saturated calomel electrode as the negative and reference electrode, respectively. The distance between each two electrodes was 2 cm. Since the GO sheets have negative charge, they moved to the positive electrode under the influence of the voltage, and deposited onto the surface of CC. Then the GO-CC samples were dried in an oven at 60 °C over night. The rGO-CC can be obtained by in-situ heated under Ar atmosphere with voltage 3 V applied on the dried GO-CC for 30 min. The hydrophobic CC was immersed in nitric acid for 1 hour and then washed with DI water and the hydrophilic CC can be obtained after dried.

Characterizations: The microstructures of these composites were characterized by a super-resolution field-emission scanning electron microscopy (JEOL JSM-7800F Prime). The surface properties of the composties were carried out on the X-ray Photoelectron Spectrometer (AXIS Ultra DLD, Kratos) and the confocal micro-Raman spectrometer (inVia Qontor). The properties of optical absorption and reflection of these composites were carried out on a Fourier Transform Infrared (FTIR) spectrometer (Nicolet 6700). The collection of the infrared photos during the experiments was done using an IR camera (MAG32, Magnity Electronics, China). The concentration of ions were tested by inductively coupled plasma optical (iCAP6300, Thermo).

Evaporation Tests: A simulated salt water solution (Ca^{2+} 9,942 mg L^{-1}, K^+ 1168 mg L^{-1}, Mg^{2+} 8,018 mg L^{-1} and Na^+ 11,210 mg L^{-1}) was prepared in a 100 mL plastic cup. One piece of porous paper

covered on a piece of polystyrene foam tightly. The heater (CC, GO-CC or rGO-CC) was binded to the top surface of the flat paper. The whole heater device can float on the water. The gap between the device and the cup was carefully closed to avoid interference. The cup together with the heater device was placed on an electronic balance, and the data of the real-time weight loss can be obtained through a computer connected with the balance.

Photothermal Power Source: The simulated solar light with diameter of 10 cm was supplied by a solar simulator (Oriel 94043 AAA, Newport). The light intensity was measured and calibrated using an optical power meter (S310C, Thorlabs Inc.).

Electrothermal Power Source: The electrical power was supplied by a DC power supply (KORAD, KA3005D/P). When using Joule heat to supply energy to realize the interfacial evaporation, both ends of the heater were adhered to the titanium foil with silver conductive glue and connected to the copper wires.

Supporting Information

Supporting Information is available from the Wiley Online Library or from the author.

References

[1] L. Zhu, M. Gao, C. K. N. Peh, X. Wang, G. W. Ho, *Adv. Energy Mater.* **2018**, *8*, 1702149.

[2] P. Zhang, J. Li, L. Lv, Y. Zhao, L. Qu, *ACS Nano* **2017**, *11*, 5087.

[3] Y. Yang, R. Zhao, T. Zhang, K. Zhao, P. Xiao, Y. Ma, P. M. Ajayan, G. Shi, Y. Chen, *ACS Nano* **2018**, *12*, 829.

[4] Y. Wang, G. Sun, J. Dai, G. Chen, J. Morgenstern, Y. Wang, S. Kang, M. Zhu, S. Das, L. Cui, L. Hu, *Adv. Mater.* **2017**, *29*, 1604257.

[5] F. Liu, L. Wang, R. Bradley, B. Zhao, W. Wu, *RSC Advances* **2019**, *9*, 29414.

[6] L. Zhu, M. Gao, C. K. N. Peh, G. W. Ho, *Nano Energy* **2019**, *57*, 507.

[7] L. Zhou, X. Li, G. W. Ni, S. Zhu, J. Zhu, *National Science Review* **2019**, *6*, 562.

[8] J. Zhou, Y. Gu, P. Liu, P. Wang, L. Miao, J. Liu, A. Wei, X. Mu, J. Li, J. Zhu, *Adv. Funct. Mater.* **2019**, 29, 1903255.

[9] M. Gao, C. K. Peh, H. T. Phan, L. Zhu, G. W. Ho, *Adv. Energy Mater.* **2018**, *8*, 1800711.

[10] L. Zhu, T. Ding, M. Gao, C. K. N. Peh, G. W. Ho, *Adv. Energy Mater.* **2019**, *9*, 1900250.

[11] F. Liu,Y. Lai, B. Zhao, R. Bradley,W. Wu, *Front. Chem. Sci. Eng.* **2019**, 13, 636-653.

[12] F. Liu, B. Zhao, W. Wu, H. Yang, Y. Ning, Y. Lai, R. Bradley, *Adv. Funct. Mater.* **2018**, *28*, 1803266.

[13] C. Celle, C. Mayousse, E. Moreau, H. Basti, A. Carella, J. P. Simonato, *Nano Research* **2012**, *5*, 427.

[14] T. Kim, Y. W. Kim, H. S. Lee, H. Kim, W. S. Yang, K. S. Suh, *Adv. Funct. Mater.* **2013**, *23*, 1250.

[15] S. Hong, H. Lee, J. Lee, J. Kwon, S. Han, Y. D. Suh, H. Cho, J. Shin, J. Yeo, S. H. Ko, *Adv. Mater.* **2015**, *27*, 4744.

[16] C. Hudaya, J. H. Park, W. C. Choi, J. K. Lee, *Symposium on Nanocrystal Embedded Dielectrics for Electronic and Photonic Devices, ECS International Meeting, Toronto, May 12-17, **2013**, 53, 161.*

[17] J. H. Kim, B. D. Ahn, C. H. Kim, K. A. Jeon, H. S. Kang, S. Y. Lee, *Thin Solid Films* **2008**, *516*, 1330.

[18] Y. H. Yoon, J. W. Song, D. Kim, J. Kim, J. K. Park, S. K. Oh, C. S. Han, *Adv. Mater.* **2007**, *19*, 4284.

[19] T. J. Kang, T. Kim, S. M. Seo, Y. J. Park, Y. H. Kim, *Carbon* **2011**, *49*, 1087.

[20] A. V. Dudchenko, C. Chen, A. Cardenas, J. Rolf, D. Jassby, *Nat. Nanotechnol.* **2017**, *12*, 557.

[21] J. Kang, H. Kim, K. S. Kim, S. K. Lee, S. Bae, J. H. Ahn, Y. J. Kim, J. B. Choi, B. H. Hong, *Nano Lett.* **2011**, *11*, 5154.

[22] C. Li, Y. T. Xu, B. Zhao, L. Jiang, S. G. Chen, J. B. Xu, X. Z. Fu, R. Sun, C. P. Wong, *J. Mater. Sci.* **2015**, *51*, 1043.

[23] T. Y. Zhang, H. M. Zhao, D. Y. Wang, Q. Wang, Y. Pang, N. Q. Deng, H. W. Cao, Y. Yang, T. L. Ren, *Nanoscale* **2017**, *9*, 14357.

[24] K. S. Novoselov, A. K. Geim, S. V. Morozov, D. Jiang, Y. Zhang, S. V. Dubonos, I. V. Grigorieva, A. A. Firsov, Science. **2004**, *306*, 666.

[25] F. Torrisi, T. Hasan, W. P. Wu, Z. P. Sun, A. Lombardo, T. S. Kulmala, G. W. Hsieh, S. J. Jung, F. Bonaccorso, P. J. Paul, D. P. Chu, and A. C. Ferrari, ACS Nano, **2012**, *6*, 2992.

[26] F. Zhao, X. Zhou, Y. Shi, X. Qian, M. Alexander, X. Zhao, S. Mendez, R. Yang, L. Qu, G. Yu, *Nat. Nanotechnol.* **2018**, *13*, 489.

[27] K. C. Yung, H. Liem, H. S. Choy, Z. C. Chen, K. H. Cheng, Z. X. Cai, *J. Appl. Phys.* **2013**, *113*.

[28] D. A. Sokolov, K. R. Shepperd, T. M. Orlando, *J. Phys. Chem. Lett.* **2010**, *1*, 2633.

[29] A. C. Ferrari, J. C. Meyer, V. Scardaci, C. Casiraghi, M. Lazzeri, F. Mauri, S. Piscanec, D. Jiang, K. S. Novoselov, S. Roth, A. K. Geim, *Phys. Rev. Lett.* **2006**, *97*, 187401.

[30] W. S. Hummers, R. E. Offeman, *J. Am. Chem. Soc.* **1958**, *80*, 1339.

A short summary and the Imagine of Table of Contents

Graphene-Carbon Composites for Solar and Low-voltage Powered Efficient Interfacial Evaporation

Fenghua Liu, Lijian Wang, Robert Bradley, Binyuan Zhao* and Weiping Wu*
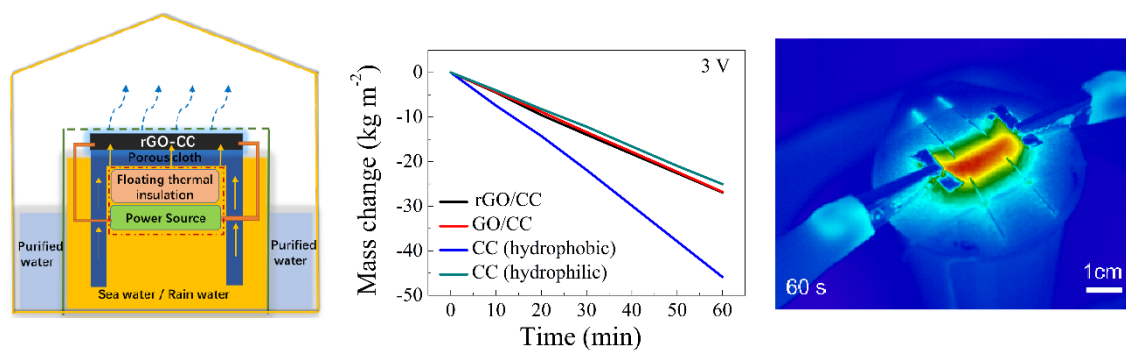
Photothermal evaporation devices with flexible ultrathin graphene-carbon cloth (CC) composites demonstrated excellent solar powered steam generation performances (2.54 kg m^{-2} h^{-1} under 1 sun illumination). The all carbon-based devices can also be operated as low voltage powered (1 V to 3 V) Joule heating elements for a wide temperature range up to 389 °C, boosting the seawater evaporation rate up to 45.87 kg m^{-2} h^{-1}.

Supporting Information

Graphene-Carbon Composites for Solar and Low-voltage Powered Efficient Interfacial Evaporation

Fenghua Liu, Lijian Wang, Robert Bradley, Binyuan Zhao* and Weiping Wu*

F. Liu, L. Wang, Prof. B. Zhao

State Key Laboratory of Metal Matrix Composites,

School of Materials Science and Engineering,

Shanghai Jiao Tong University,

Shanghai, 200240, China

Prof. R. Bradley

Department of Materials, University of Oxford,

16 Parks Road, Oxford, OX1 3PH, United Kingdom,

MatSurf Technology Ltd.

The Old Stables Marion Lodge, Little Salkeld, Penrith,

Cumbria, CA10 1NW, United Kingdom

Dr. W. Wu

Department of Electrical and Electronic Engineering,

School of Mathematics, Computer Science and Engineering,

City, University of London,

Northampton Square, London, EC1V 0HB, United Kingdom
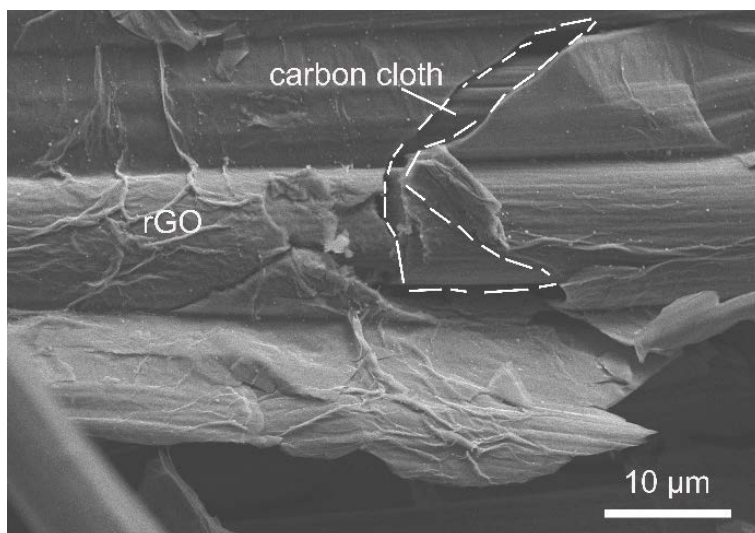

Corresponding Authors

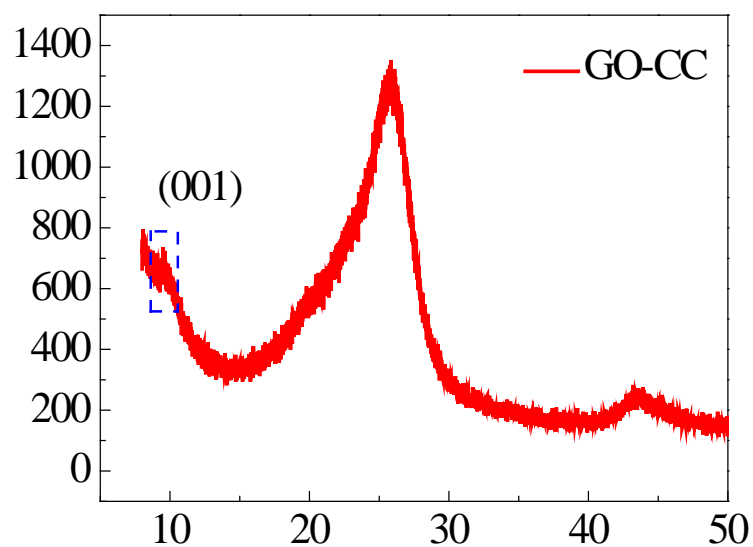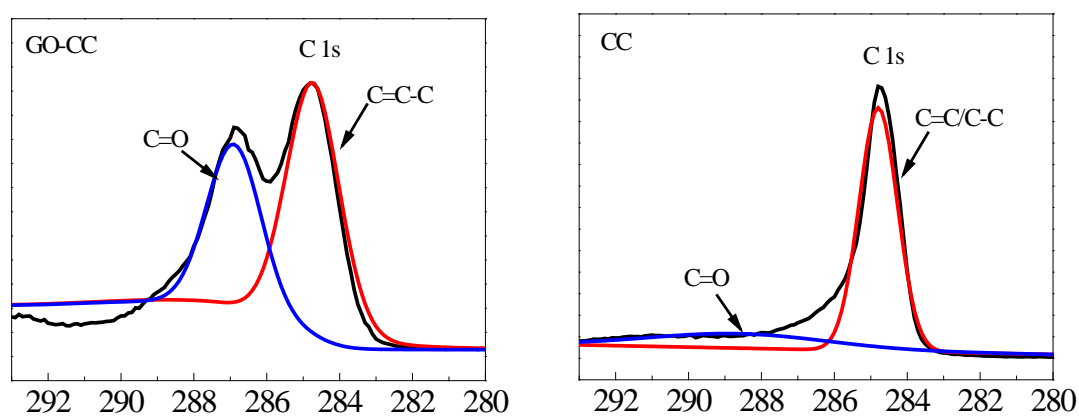*Email: byzhao@sjtu.edu.cn

*Email: Weiping.Wu@city.ac.uk

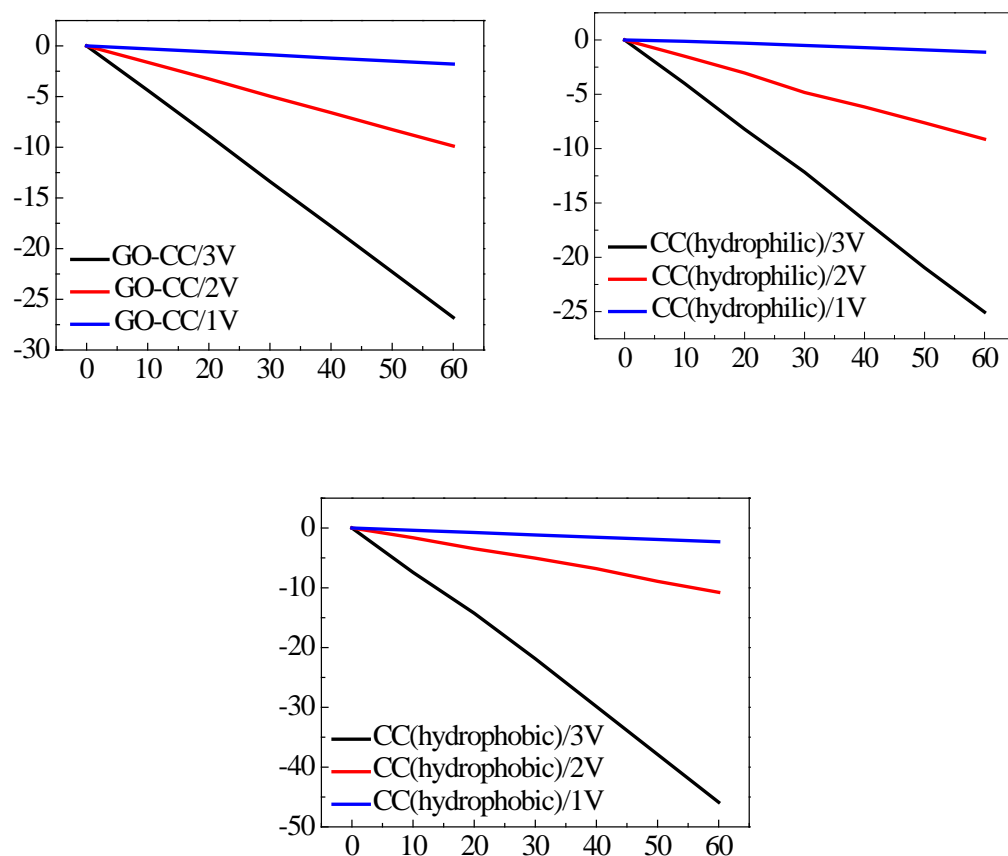**Figure S1.** An optical photograph of GO deposited on a piece of carbon cloth (CC).

Figure S2. Scanning electron microscope (SEM) image of the Graphene oxide on a piece of carbon cloth, forming the GO-CC composite.
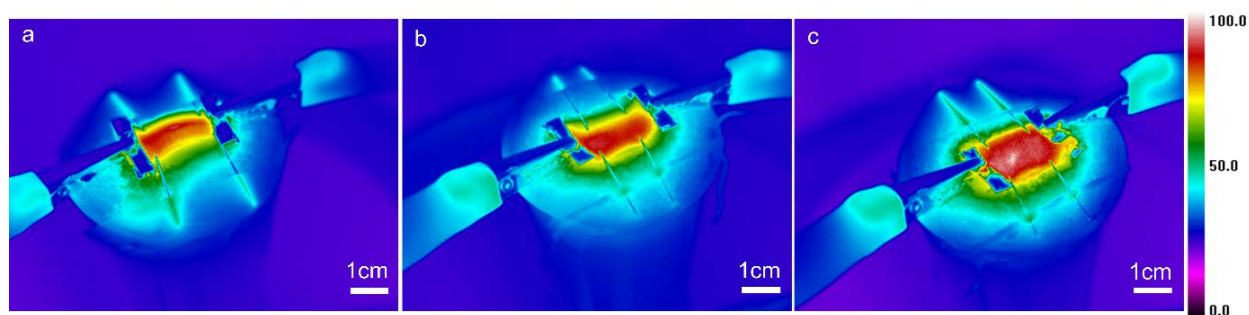
Figure S3. The X-ray diffraction (XRD) pattern of the GO-CC sample.


Figure S4. The X-ray photoelectron spectroscopy (XPS) spectrum of a) a GO-CC sample, b) a piece of CC sample.

Figure S5. The mass change as a function of time under different applied voltages of a) GO-CC, b) CC (hydrophilic), c) CC (hydrophobic) heaters.
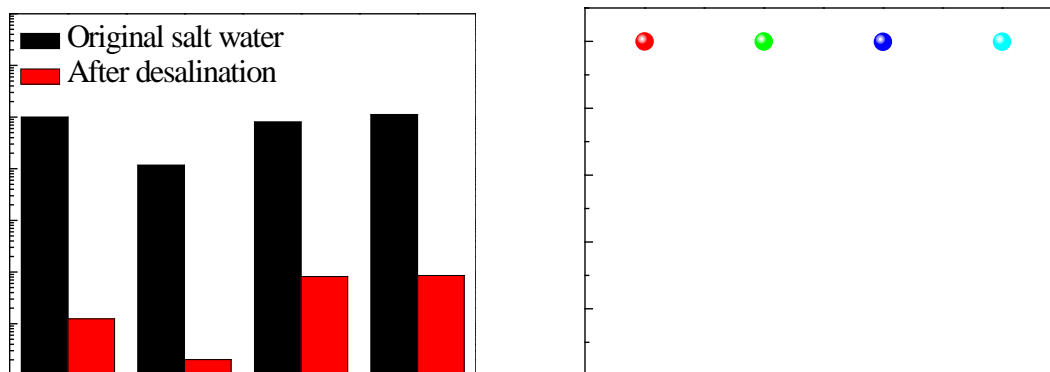

Figure S6. The infrared (IR) camera photos in steady states under the same applied voltage (3 V) of **a**, GO-CC, **b**, rGO-CC and **c**, CC (hydrophobic) heaters.
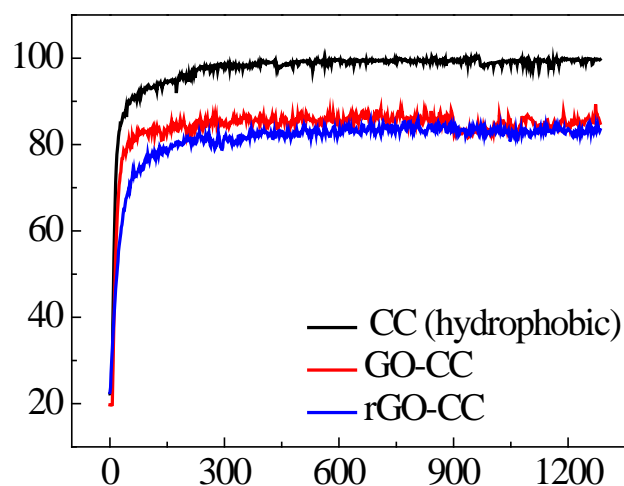
Figure S7. The change surface temperature as a function of time of the devices under a applied voltage of 3 V.
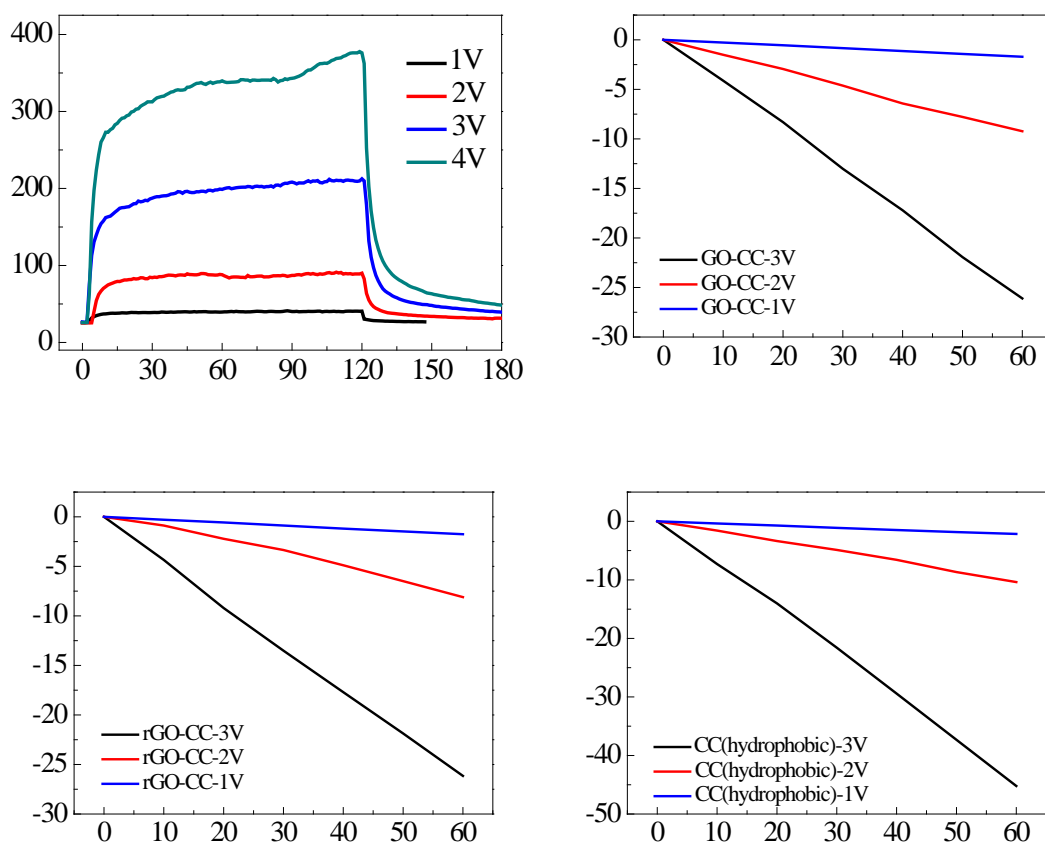
Figure S8. The electric thermal and interfacial evaporation performances (sample size 4×2 cm).

Figure S9. a) The concentration of the primary ions in a salt water sample before and after desalination. b) The ion rejection of salt water sample undergoing the desalination.

Table S1. The energy conversion of different Joule heating evaporation elements

Material	Voltage (V)	Power (W)	Mass change (g)	η (%)
CC (hydrophobic)	3	9.804	11.01	80.2
	2	3.16	2.58	58.3
	1	0.66	0.55	59.5
GO-CC	3	6.14	6.43	74.8
	2	2.656	2.37	63.7
	1	0.545	0.43	56.3
rGO-CC	3	6.46	6.46	71.4
	2	2.376	1.93	58.0
	1	0.518	0.42	57.9